Predecision for Wideband Spectrum Sensing With Sub-Nyquist Sampling

Tianyi Xiong, *Member, IEEE*, Hongbin Li, *Senior Member, IEEE*, Peihan Qi, Zan Li, *Senior Member, IEEE*, and Shilian Zheng, *Member, IEEE*

***Abstract*—Built on compressed sensing theories, sub-Nyquist spectrum sensing (SNSS) has emerged as a promising solution to the wideband spectrum sensing problem. However, most of the existing SNSS methods do not distinguish if primary users (PUs) are present or absent in the concerned spectrum band and directly pursue support recovery of the PUs. This may lead to a high false alarm rate and a waste of computational cost. To address the issue, we propose a predecision algorithm, referred to as the pairwise channel energy ratio (PCER) detector, to determine the presence or absence of PUs prior to signal support recovery. The proposed detector is based on the popular modulated wideband converter (MWC) framework for SNSS, which has several advantages over other SNSS approaches. The PCER test statistic is constructed from compressed samples obtained by the MWC. The decision threshold and the detection probability are derived in closed form following the Neyman–Pearson criterion. Numerical results are presented to verify the theoretical calculation. The proposed PCER detection method is shown to be able to detect the existence of PUs in a wide range of signal-to-noise ratio, while being robust to noise uncertainty and does not need the prior knowledge of the PU signals. Additionally, our results show that the use of the PCER detector leads to a significant improvement of the correct support recovery rate of the PU signals.**

***Index Terms*—Cognitive radio (CR), compressed sampling, correct support recovery (CSR), modulated wideband converter (MWC), noise uncertainty, sub-Nyquist spectrum sensing (SNSS), wideband spectrum sensing.**

I. Introduction

THE exponential growth of ubiquitous wireless devices and services during past decades has imposed increasing stress on the limited spectrum resources. The current spectrum policy, primarily based on allocating a fixed-frequency band to individual wireless services, has been shown to be highly inefficient, causing congestion in some bands while underutilization in others [1]–[3]. The cognitive radio (CR) [4]–[6], which allows secondary users (SUs) to opportunistically access unused radio spectrum, called white space, has been widely considered as a promising solution to the above problem. A key function in the CR is spectrum sensing that involves monitoring the spectrum usage and detecting the presence/absence of primary users (PUs) [7]–[9]. Recently, wideband spectrum sensing has received significant interest [10]–[13], where SUs perform spectrum sensing in a wide range of frequency band to search for more access opportunities. However, the implementation of wideband spectrum sensing at the SU has some difficulties, e.g., the need for a complex front end, high sampling rate, and fast digital signal processing [14]. Meanwhile, compressed sensing has been established as a new field that offers powerful tools for recovering sparse signals from a few nonadaptive linear measurements, significantly reducing the sampling rate compared with the conventional Nyquist sampling framework [15]–[18]. This has motivated the interest of using compressed sensing techniques to solve the wideband spectrum sensing problem.

Sub-Nyquist spectrum sensing (SNSS) based on compressed sampling has been considered in a multitude of studies. In [19], a wideband spectrum sensing approach based on Nyquist sampling is introduced by using sparsity recovery techniques originated from compressed sensing. The authors of [20] proposed an autonomous compressed spectrum sensing algorithm based on a measurement procedure and the validation approach. Qin *et al.* [21] combine compressive spectrum sensing with geolocation database to find spectrum holes in the CR. For compressed sampling of wideband signals, an analog-to-information converter (AIC) that employs a wideband pseudorandom demodulator and a low-rate sampler was introduced in [22]–[25]. Based on the AIC, several SNSS methods consisting of two stages were proposed in [26]–[29]. In the first stage, the original wideband signal or its power spectrum is reconstructed from compressed samples; in the second stage, wideband spectrum sensing is performed to determine the locations of the occupied frequency bands. However, it has been found that the AIC framework can be affected by some input signal model mismatch problems [10], [30]. Multicoset sampling is another compressed sampling framework [10], [31]–[33], which uses multiple analog-to-digital converter (ADCs) in a time inter-

Manuscript received June 13, 2016; revised October 23, 2016 and December 15, 2016; accepted January 6, 2017. Date of publication January 23, 2017; date of current version August 11, 2017. This work was supported by the National Natural Science Foundation of China under Grant 61501356 and Grant 61471395. The work of H. Li was supported in part by the National Science Foundation under Grant ECCS-1408182 and Grant ECCS-1609393. The review of this paper was coordinated by Prof. S.-H. Leung. *(Corresponding author: Peihan Qi.)*

T. Xiong, P. Qi, and Z. Li are with the State Key Laboratory of Integrated Service Networks, Xidian University, Xi'an 710071, China (e-mail: xiongtianyi1989@163.com; phqi@xidian.edu.cn; zanli@xidian.edu.cn).

H. Li is with the Department of Electrical and Computer Engineering, Stevens Institute of Technology, Hoboken, NJ 07030 USA (e-mail: Hongbin.Li@stevens.edu).

S. Zheng is with the Science and Technology on Communication Information Security Control Laboratory, Jiaxing 314033, China (e-mail: lianshizheng@126.com).

Color versions of one or more of the figures in this paper are available online at http://ieeexplore.ieee.org.

Digital Object Identifier 10.1109/TVT.2017.2656940

leaving fashion. However, maintaining accurate time shifts and channel synchronization between sampling channels are difficult to implement, and the possible front ends are far below the wideband regime.

A practical compressed sampling framework based on a modulated wideband converter (MWC) is proposed to cope with the input model mismatch problem [30], [34]. The MWC framework describes the input signals as a sparse union of shift-invariant subspaces and processes the input signal in multiple channels simultaneously. In each channel, the input signal is multiplied by a periodic ± 1 sequence, filtered by a low-pass filter (LPF), and then sampled by a low-rate ADC. By means of frame construction and solving a multiple measurement vector problem, the signal support can be estimated directly without a full signal recovery. It has been shown that the MWC-based SNSS has the advantages of being able to adaptive to different types of signals, fast signal support recovery (SR), and low computational load [35].

Most of the existing SNSS methods are developed under the assumption that the PU signals are present in the concerned frequency band. However, there are cases where the frequency band may be completely vacant and only background noise exists, e.g., in satellite and millimeter wave communications [2], [3], [36]. In such cases, a direct application of the aforementioned SNSS methods is inappropriate, due to the absence of a sparse signal, and would lead to several problems: 1) high false alarm rate—SNSS methods are likely to provide incorrect spectrum sensing results, causing a high false alarm probability and making the vacant spectrum bands to be underutilized; and 2) a waste of computational cost and energy.

In this paper, we propose a predecision algorithm, referred to as the pairwise channel energy ratio (PCER) detector, which is integrated with the MWC framework for SNSS. The PCER algorithm is to determine the presence/absence of PU signals prior to signal SR. Only if the PU signals are detected in the concerned frequency band, the function of signal SR will be activated to estimate the location of the occupied bands; otherwise, signal SR is bypassed. It is necessary to point out that the proposed predecision algorithm can also be extended to other compressed sampling framework besides the MWC. We model this predecision problem as a binary hypothesis testing and construct a test statistic with compressed samples to detect the PU signals. By exploiting the statistical properties of the test statistic, we derive the decision threshold and the probability of detection in closed form, following the Neyman–Pearson (NP) criterion.

Theoretical derivation and numerical simulation show that our PCER detector is robust to noise uncertainty [37]. Furthermore, it does not require any prior knowledge of the PU signal. Some spectrum sensing techniques have been proposed to overcome noise uncertainty [6], [38]–[40]. The algorithms proposed in [6] and [38] employ the covariance matrix of the signal samples, and eigenvalue decomposition is required. The cyclostationarity-based spectrum sensing in [39] needs to know the cyclic frequency of the signal as a prior knowledge; otherwise, exhaustive search has to be carried out. In recent work of Sun *et al.* [40], particle filtering technology is used to design a spectrum sensing technique to overcome noise uncertainty.

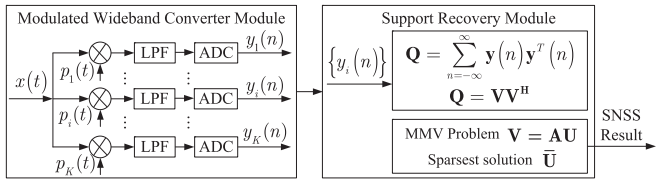

Fig. 1. Conventional MWC-based SNSS.

However, the above-mentioned spectrum sensing algorithms are designed in the conventional Nyquist sampling framework and are not suitable for the MWC-based SNSS framework in this paper. With the PECR predecision algorithm, the presence/absence of PU signals is determined before signal SR, which avoids unnecessary computational overhead and high false alarm probability caused by incorrect SR. As a result, the functions of compressed sampling, signal detection, and signal recovery are integrated, making the SNSS more useful for wideband spectrum sensing.

The rest of this paper is organized as follows. Section II briefly reviews the MWC-based SNSS framework and introduces the predecision problem concerned in this paper. In Section III, the PCER algorithm is summarized, and closed-form expressions of the decision threshold and probability of detection are derived. Section IV provides numerical results and discussions on the performance of the proposed algorithm. The whole work is concluded in Section V.

Notation: $E[\cdot]$ and $D[\cdot]$ represent the mathematical expectation and variance operator, respectively, $\mathrm{Cov}[\cdot,\cdot]$ denotes the covariance between two random variables, and $\Re[\cdot]$, $\Im[\cdot]$ represent taking the real part and imaginary part, respectively.

II. MWC-Based SNSS and the Problem

To motivate the proposed algorithm and facilitate its presentation, we first briefly review the MWC-based SNSS framework and then introduce the predecision problem concerned in this paper.

A. MWC-Based SNSS

Fig. 1 shows the conventional MWC-based SNSS [35], which consists of the MWC sampling module and the SR module. The former converts the input analog signal $x(t)$ into compressed samples, and the latter estimates the support of the PU signals. At the SU, the received signal $x(t)$, which is bandlimited in the range of $[-f_{\mathrm{NYQ}}/2, f_{\mathrm{NYQ}}/2]$, is fed to K channels of the MWC module simultaneously. The signal in the ith channel is multiplied by a T_p-periodic sequence $p_i(t)$, which contains M chips alternating between levels ± 1. Specifically

$$p_i(t) = \theta_{im} \quad m\frac{T_p}{M} \le t \le (m+1)\frac{T_p}{M},\ 0 \le m \le M-1 \tag{1}$$

where $\theta_{im} \in \{-1, +1\}$ and $p_i(t + T_p) = p_i(t)$. Afterward, the mixed signal of each channel is filtered by an LPF $h(t)$ with pass band $[-f_s/2, f_s/2]$, where f_s is the sampling rate of the subsequent low-rate ADCs. Thus, the output of the LPF is

expressed as

$$y_i(t) = \int_{-\infty}^{\infty} x(\tau)\, p_i(\tau)\, h(t-\tau)\, d\tau \tag{2}$$

where $i = 1, 2, \ldots, K$. Discretizing $y_i(t)$ with a sampling interval $T_s = 1/f_s$ yields

$$y_i(n) = y_i(t)|_{t=nT_s}, \quad n = 0, 1, 2 \ldots. \tag{3}$$

The discrete-time Fourier transform (DTFT) of $y_i(n)$ is given by [30]

$$\begin{aligned} Y_i\left(e^{j2\pi f T_s}\right) &= \sum_n y_i(n) e^{-j2\pi f n T_s} \\ &= \sum_{l=-L_0}^{L_0} c_{il} X(f - l f_p), \quad f \in \mathcal{F} \end{aligned} \tag{4}$$

where $c_{il} = \frac{1}{T_p}\int_0^{T_p} p_i(t) e^{-j\frac{2\pi}{T_p} lt} dt$ are the Fourier series coefficients of $p_i(t)$, $f_p = 1/T_p$, $X(f)$ is the Fourier transform of $x(t)$, and $L_0 = \lceil (f_{\text{NYQ}} + f_s)/(2f_p) \rceil - 1$ is chosen as the smallest integer such that the summation in (4) contains all the nonzero subbands of $X(f)$, which are aliased into $\mathcal{F} = [-f_s/2, f_s/2]$. Equation (4) is key to the SR of the input signal, since it relates $x(t)$ to the DTFT of observations $y_i(n)$, which are obtained from sub-Nyquist sampling.

Define $\mathbf{Y}(f) = [Y_1(f), \ldots, Y_i(f), \ldots, Y_K(f)]^T$, with $Y_i(f) = Y_i\left(e^{j2\pi f T_s}\right)$ and $\mathbf{Z}(f) = [Z_1(f), \ldots, Z_l(f), \ldots, Z_L(f)]^T$, with $Z_l(f) = X(f + (l - L_0 - 1) f_p)$, where $L = 2L_0 + 1$. Consequently, (4) can be rewritten in a more compact form as

$$\mathbf{Y}(f) = \mathbf{A}\mathbf{Z}(f) \tag{5}$$

where $f \in \mathcal{F}$, and $\mathbf{A} \in \mathbb{C}^{K \times L}$ with elements $\mathbf{A}_{il} = c_{i,-l+L_0+1}$, $1 \le i \le K$ and $1 \le l \le L$. It is necessary to point out that if $x(t)$, in the absence of noise, is a sparse multiband signal, i.e., there are a few nonzeros bands in the frequency domain, $\mathbf{Z}(f)$ has the same sparsity support as $x(t)$. This is because each element of $\mathbf{Z}(f)$ corresponds to one subband of $X(f)$ that is shifted into $[-f_s/2, f_s/2]$. Without loss of generality, we set $f_p = f_s$ in this paper, and L equals M under this setting [34].

To implement SR with compressed measurements $y_i(n)$, consider the autocorrelation matrix of $\mathbf{Y}(f)$

$$\mathbf{Q} = \int_{-f_s/2}^{+f_s/2} \mathbf{Y}(f)\mathbf{Y}^H(f)\, df = \sum_{n=-\infty}^{\infty} \mathbf{y}(n)\mathbf{y}^T(n) \tag{6}$$

where $\mathbf{y}(n) = [y_1(n), \ldots, y_i(n), \ldots, y_K(n)]^T$ is the compressed samples output from all the channels of the MWC at time instance nT_s. Decompose the autocorrelation matrix as $\mathbf{Q} = \mathbf{V}\mathbf{V}^H$, where $\mathbf{V}$ is the Hermitian square root of $\mathbf{Q}$. It is shown that the following MMV sparse recovery problem [33]

$$\mathbf{V} = \mathbf{A}\mathbf{U} \tag{7}$$

has a unique sparsest solution $\bar{\mathbf{U}}$ with the fewest nonzero rows. If $x(t)$ is a sparse multiband signal, the support of vector $\mathbf{Z}(f)$ can be obtained as $\mathbb{S} = \text{supp}\left(\bar{\mathbf{U}}\right)$. As a result, the number and location of occupied bands by PUs can be estimated.

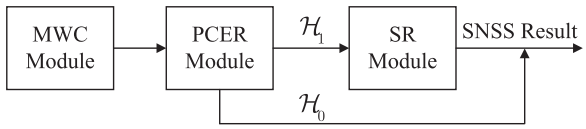

Fig. 2. Proposed MWC-based SNSS framework.

However, if the frequency band is vacant and $x(t)$ contains only white noise, the support of $\bar{\mathbf{U}}$ solved from (7) is totally irrelevant (note that the support of $\mathbf{Z}(f)$ does not even exist in this case). This implies that the SR in the conventional MWC-based SNSS will lead to incorrect spectrum sensing results, causing a high false alarm rate and unnecessary computational expenses. Clearly, there is no need to perform SR if the frequency band is empty.

B. Problem

To address the above issue, we propose to insert a predecision module, referred to as the PCER in this paper, between the MWC module and the SR module, as sketched in Fig. 2, where $\mathcal{H}_0$ denotes the hypothesis that there is only white noise in the input signal and $\mathcal{H}_1$ represents that there exist PU signals. If the detection result of the PCER module is $\mathcal{H}_0$, indicating that the whole frequency band is available and the SR is unnecessary and the SR module is bypassed. On the other hand, if the PCER module decides hypothesis $\mathcal{H}_1$, SR is conducted subsequently, and the location of the occupied bands is estimated. By adding the PCER module, the proposed framework integrates the functions of data acquisition, detection, and estimation, making the MWC-based SNSS more useful for wideband spectrum sensing.

As shown in Fig. 2, the PCER module has to solve the following binary hypothesis detection problem based on compressed samples:

$$y_i(n) = \begin{cases} w_i(n), & \mathcal{H}_0 \\ s_i(n) + w_i(n), & \mathcal{H}_1 \end{cases} \tag{8}$$

where $i = 1, 2, \ldots, K$, $w_i(n)$ is the noise sample output from the ith channel of the MWC produced by a zero-mean Gaussian white noise $w(t)$ at the input with power spectrum density σ_w^2, and $s_i(n)$ is the signal sample produced by $s(t)$ at the input which is sparse and composed of one or more PU signals.

The detection performance is evaluated by the probability of detection P_d and the probability of false alarm P_f, which are defined as

$$P_d = \Pr\{\text{decision} = \mathcal{H}_1 | \mathcal{H}_1\} \tag{9a}$$

$$P_f = \Pr\{\text{decision} = \mathcal{H}_1 | \mathcal{H}_0\} \tag{9b}$$

where P_d is the probability of detecting the PU sparse signal in the concerned frequency band when it is present, and P_f is the probability that the detector incorrectly decides that the considered frequency band is occupied, whereas there is only white noise.

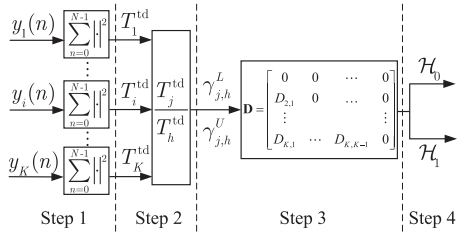

Fig. 3. PCER Module.

III. Proposed PCER Detector and Performance Analysis

In this section, we first present the proposed PCER predecision algorithm. Afterward, we study the statistical characteristics of the PCER detector under both hypothesis $\mathcal{H}_0$ and $\mathcal{H}_1$. Finally, closed-form expressions of the decision threshold and the detection probability of the PCER detector are derived under the NP criterion.

A. PCER Detector

For the binary hypothesis detection problem (8), we construct a test statistic with the compressed measurements $\mathbf{y}(n)$ and compare it with a decision threshold to provide a decision. The problem can be solved by the energy detector (ED), which is a widely used technique because of simplicity and low computational cost, on a channel-by-channel fashion. Nevertheless, the decision threshold of the ED depends on the background noise power, which makes its performance sensitive to any uncertainty of the noise power. There are some work investigating the ED under noise uncertainty [41]–[43], which requires estimating the noise power. Inaccurate estimation of the noise power will also affect the performance of the ED, which makes such methods not suitable for the MWC-based SNSS framework. In the following, we propose a novel test statistic, which does not require the prior knowledge of the noise power and is shown to be robust to the noise uncertainty while has a similar complexity as the ED. Formally, as shown in Fig. 3, the proposed PCER predecision algorithm is summarized as follows.

Step 1: The N-point energy T_i^{td} of the output of the ith channel of the MWC module is computed as

$$T_i^{\text{td}} = \sum_{n=0}^{N-1} |y_i(n)|^2 \tag{10}$$

where $i = 1, 2, \ldots, K$ denotes the channel index, and the superscript td represents the time domain.

Step 2: Considering the impact of noise uncertainty on the performance of ED, branch test statistics $r_{j,h}$ are constructed as PCERs

$$r_{j,h} = T_j^{\text{td}} / T_h^{\text{td}} \tag{11}$$

where $j = 2, 3, \ldots, K$ and $h = 1, 2, \ldots, j-1$. Note that the test statistics employ the compressed samples from all the K channels of the MWC.

Step 3: Since energy ratio is employed as test statistic, it is reasonable to compare $r_{j,h}$ with a lower threshold $\gamma_{j,h}^L$ and an upper threshold $\gamma_{j,h}^U$ (to be determined) to achieve better performance. As a result, a decision matrix $\mathbf{D}$ is constructed with elements given by

$$D(j,h) = \begin{cases} 0, & \text{if } \gamma_{j,h}^L < r_{j,h} < \gamma_{j,h}^U \\ 1, & \text{otherwise} \end{cases} \tag{12}$$

where $j = 2, 3, \ldots, K$, $h = 1, 2, \ldots, j-1$, and $D(j,h)$ is the element of $\mathbf{D}$ in the jth row and the ith column. For other values of j and h, $D(j,h)$ is regarded as irrelevant and set to 0. Note that there are $(K^2 - K)/2$ relevant elements in the decision matrix $\mathbf{D}$.

Step 4: Given the branch decision results (i.e., the relevant elements of $\mathbf{D}$), there are several popular fusion rules, e.g., the "OR," "AND," and "K-out-of-N" rule [44]–[46], which can be used to obtain the final decision result. For simplicity, we use the "OR" rule in this paper, and the other rules can be easily accommodated. Therefore, the final decision result is obtained as

$$\begin{cases} \sum_{j=2}^{K} \sum_{h=1}^{j-1} D(j,h) = 0, & \text{decide } \mathcal{H}_0 \\ \sum_{j=2}^{K} \sum_{h=1}^{j-1} D(j,h) \geq 1, & \text{decide } \mathcal{H}_1. \end{cases} \tag{13}$$

For a single pair of valid j and h, we referred to $P_f^{j,h}$ and $P_d^{j,h}$ as the branch probability of false alarm and the branch probability of detection, respectively, which are defined as

$$P_f^{j,h} = \Pr\left\{ r_{j,h} \leq \gamma_{j,h}^L || r_{j,h} \geq \gamma_{j,h}^U | \mathcal{H}_0 \right\} \tag{14a}$$

$$P_d^{j,h} = \Pr\left\{ r_{j,h} \leq \gamma_{j,h}^L || r_{j,h} \geq \gamma_{j,h}^U | \mathcal{H}_1 \right\} \tag{14b}$$

where $||$ denotes the logic "or" operator.

Note that (13) uses all branch ratios in (11) to determine the final decision, which is called all-branch fusion rule in the following. It is clear to see that these ratios are statistically correlated with each other, since some of the ratios share the same nominator and denominator, which can cause some deviation if we directly applying the "OR" fusion equation that requires independent fusion branches [46].

However, we found that, via numerical simulation, there is relatively small correlation among the branch ratios $r_{j,j-1}$, $j = 2, 3, \ldots, K$, for which the "OR" fusion equation can be applied with only slight mismatch between theoretical and simulation results. Also, we define $r_{1,0}$ as $T_1^{\text{td}}/T_K^{\text{td}}$, which also has small correlation with the above branch ratios. The corresponding $\gamma_{1,0}^L$, $\gamma_{1,0}^U$, and $D(1,0)$ are also defined in the same way as before. Therefore, similar to (13), we have

$$\begin{cases} \sum_{j=1}^{K} D(j, j-1) = 0, & \text{decide } \mathcal{H}_0 \\ \sum_{j=1}^{K} D(j, j-1) \geq 1, & \text{decide } \mathcal{H}_1 \end{cases} \tag{15}$$

and the overall probability of false alarm and detection are given by

$$P_f = 1 - \prod_{j=1}^{K} (1 - P_f^{j,j-1}) \tag{16a}$$

$$P_d = 1 - \prod_{j=1}^{K} (1 - P_d^{j,j-1}). \tag{16b}$$

We should point out that the decision rule (15) only uses partial branch ratios defined in (11), which is called partial-branch fusion rule in the following, while the decision rule (13) uses all branch ratios that could achieve better performance at higher complexity. Thus, by providing both detectors, a tradeoff between performance and complexity is possible.

To find the overall P_f and P_d in (16), we should first study the statistical property of $r_{j,h}$ under both hypotheses, which is examined in the following subsections, and then use (14) to find the branch probability $P_f^{j,h}$ and $P_d^{j,h}$. It is important to point out that the above algorithm is not limited to the MWC-based sampling framework and can easily be extended to other compressed sampling frameworks.

B. False Alarm Probability Analysis

Under $\mathcal{H}_0$, the received signal $x(t)$ contains only white noise. Following the NP criterion, we set a target branch probability of false alarm $P_f^{j,h}$ and then find the branch threshold $\gamma_{j,h}^L$ and $\gamma_{j,h}^U$, $j = 1, 2, \ldots, K$, $h = j - 1$, which is given by the following theorem.

Theorem 1: For a given target branch probability of false alarm $P_f^{j,h}$, the corresponding branch threshold of the detector (11) is given by (17a) and (17b) at the bottom of this page, where $\Phi^{-1}(x)$ is the inverse function of the Gaussian cumulative distribution function (CDF) $\Phi(x) = \frac{1}{\sqrt{2\pi}} \int_{-\infty}^{x} e^{-\frac{\eta^2}{2}} d\eta$, N is the number of compressed measurements used to compute the channel energy and

$$\rho_{\mathcal{H}_0}^{j,h} \triangleq \left(\rho_0^2 + \rho_1^2 + \rho_2^2 + \rho_3^2\right)/2 \tag{18}$$

where

$$\rho_0 = \sum_{l=-L_0}^{L_0} \left[\Re(c_{jl})\Im(c_{hl}) - \Re(c_{hl})\Im(c_{jl})\right] \tag{19a}$$

$$\rho_1 = \sum_{l=-L_0}^{L_0} \left[\Im(c_{jl})\Re(c_{hl}) - \Re(c_{jl})\Im(c_{hl})\right] \tag{19b}$$

$$\rho_2 = \sum_{l=-L_0}^{L_0} \left[\Re(c_{jl})\Re(c_{hl}) + \Im(c_{hl})\Im(c_{jl})\right] \tag{19b}$$

$$\rho_3 = \sum_{l=-L_0}^{L_0} \left[\Re(c_{jl})\Re(c_{hl}) + \Im(c_{hl})\Im(c_{jl})\right]. \tag{19c}$$

Proof: To prove Theorem 1, we start from (14a), which requires the statistical property of $r_{j,h}$ defined in (11). Note that the branch test statistic $r_{j,h}$ is the ratio of the signal energy from two different channels of the MWC module. We first need to determine the statistical property of the numerator and denominator, i.e., the channel energy T_j^{td} and T_h^{td}, respectively.

Considering the Parseval theorem that the energy in the time domain can be equivalently computed in the frequency domain, we use the channel energy T_j^{fd} and T_h^{fd} instead of T_j^{td} and T_h^{td}, respectively, where the superscript fd represents the frequency domain. It is more convenient to carry out the analysis and computation in the frequency domain. Specifically, by the Parseval theorem,

$$T_i^{\text{fd}} = \frac{1}{N} \sum_{k=0}^{N-1} |Y_i(k)|^2 = \sum_{n=0}^{N-1} |y_i(n)|^2 = T_i^{\text{td}} \tag{20}$$

where $Y_i(k), i = 1, 2, \ldots, K,\ k = 0, 1, \ldots, N-1$, are the discrete Fourier transform (DFT) of $y_i(n)$. Since the DFT of $y_i(n)$ is obtained by uniformly sampling the DTFT of $y_i(n)$, which is given by (4), $Y_i(k)$ under $\mathcal{H}_0$ is

$$Y_i(k) = \sum_{l=-L_0}^{L_0} c_{il} X(k - lN) = \sum_{l=-L_0}^{L_0} c_{il} W(k - lN) \tag{21}$$

where $W(k - lN)$ is the DFT of the additive Gaussian white noise $w(t)$ at the input of the SU.

Lemma 1 in Appendix A indicates that T_i^{fd} is a sum of N independent random variables $|Y_i(k)|^2, k = 0, 1, 2, \ldots, N-1$, with identical mean and variance under $\mathcal{H}_0$. Thus, for large N and following the central limit theorem, T_i^{fd} is approximately a Gaussian variable with mean and variance given by

$$E\left[T_i^{\text{fd}}|\mathcal{H}_0\right] = \frac{1}{N} \sum_{k=0}^{N-1} E\left[|Y_i(k)|^2\right] = N\sigma_w^2 \tag{22a}$$

$$D\left[T_i^{\text{fd}}|\mathcal{H}_0\right] = \frac{1}{N^2} \sum_{k=0}^{N-1} D\left[|Y_i(k)|^2\right] = N\sigma_w^4. \tag{22b}$$

The covariance of two different channel energies is

$$\begin{aligned} \text{Cov}\left[T_j^{\text{fd}}, T_h^{\text{fd}}\right] &= \text{Cov}\left[\frac{1}{N}\sum_{k=0}^{N-1} |Y_j(k)|^2, \frac{1}{N}\sum_{k=0}^{N-1} |Y_h(k)|^2\right] \\ &= \frac{1}{N^2}\left[\sum_{k=0}^{N-1}\left(\text{Cov}\left[|Y_j(k)|^2, |Y_h(k)|^2\right]\right)\right] \\ &= \frac{N\sigma_w^4}{2}\left(\rho_0^2 + \rho_1^2 + \rho_2^2 + \rho_3^2\right) \end{aligned} \tag{23}$$

$$\gamma_{j,h}^L = \frac{N - \rho_{\mathcal{H}_0}^{j,h}\left[\Phi^{-1}\left(P_{f,L}^{j,h}\right)\right]^2 - \Phi^{-1}\left(P_{f,L}^{j,h}\right)\sqrt{\left(\left(\rho_{\mathcal{H}_0}^{j,h}\right)^2 - 1\right)\left(\left[\Phi^{-1}\left(P_{f,L}^{j,h}\right)\right]^2\right) + 2N\left(\rho_{\mathcal{H}_0}^{j,h} - 1\right)}}{N - \left[\Phi^{-1}\left(P_{f,L}^{j,h}\right)\right]^2} \tag{17a}$$

$$\gamma_{j,h}^U = \frac{N - \rho_{\mathcal{H}_0}^{j,h}\left[\Phi^{-1}\left(1 - P_{f,U}^{j,h}\right)\right]^2 + \Phi^{-1}\left(1 - P_{f,U}^{j,h}\right)\sqrt{\left(\left(\rho_{\mathcal{H}_0}^{j,h}\right)^2 - 1\right)\left(\left[\Phi^{-1}\left(1 - P_{f,U}^{j,h}\right)\right]^2\right) + 2N\left(\rho_{\mathcal{H}_0}^{j,h} - 1\right)}}{N - \left[\Phi^{-1}\left(1 - P_{f,U}^{j,h}\right)\right]^2} \tag{17b}$$

where ρ_0, ρ_1, ρ_2, and ρ_3 are defined in Theorem 1. The last equality of (23) follows from (39) of Lemma 1. Therefore, the correlation coefficient $\rho_{\mathcal{H}_0}^{j,h}$ between T_j^{fd} and T_h^{fd} can be calculated as

$$\rho_{\mathcal{H}_0}^{j,h} = \frac{\text{Cov}\left[T_j^{\text{fd}}, T_h^{\text{fd}}\right]}{\sqrt{D\left[T_j^{\text{fd}}|\mathcal{H}_0\right] D\left[T_h^{\text{fd}}|\mathcal{H}_0\right]}} = \frac{\left(\rho_0^2+\rho_1^2+\rho_2^2+\rho_3^2\right)}{2}. \tag{24}$$

According to the derivation above, it shows that $r_{j,h}$ under $\mathcal{H}_0$ is the ratio of two statistically correlated Gaussian variables whose statistics are given by (22)–(24). Furthermore, to find the CDF of $r_{j,h}$, we employ the following property.

Property 1 (see [47]): The ratio R of two statistically correlated Gaussian random variable Z_1 and Z_2 obeys the distribution with the following CDF:

$$F_R(r) = \Pr(R<r) = \Phi\left(\frac{r\mu_2-\mu_1}{\sqrt{\sigma_1^2-2r\rho\sigma_1\sigma_2+r^2\sigma_2^2}}\right) \tag{25}$$

where $\Phi(x)$ is defined in Theorem 1, μ_1, μ_2, σ_1^2, and σ_2^2 are the mean and variance of Z_1 and Z_2, respectively, and ρ is the correlation coefficient of Z_1 and Z_2.

To apply Property 1 to the branch test statics defined in (11), we first split the branch $P_f^{j,h}$ into two parts as lower part $P_{f,L}^{j,h}$ and upper part $P_{f,U}^{j,h}$ according to (14), which satisfy

$$P_{f,L}^{j,h} = \Pr\left(r_{j,h} \le \gamma_{j,h}^L|\mathcal{H}_0\right) \tag{26a}$$

$$P_{f,U}^{j,h} = \Pr\left(r_{j,h} \ge \gamma_{j,h}^U|\mathcal{H}_0\right). \tag{26b}$$

Applying Property 1 to above equations yields

$$P_{f,L}^{j,h} = \Phi\left(\frac{\sqrt{N}\gamma_{j,h}^L-\sqrt{N}}{\sqrt{1-2\gamma_{j,h}^L\rho_{\mathcal{H}_0}^{j,h}+(\gamma_{j,h}^L)^2}}\right) \tag{27a}$$

$$P_{f,U}^{j,h} = 1-\Phi\left(\frac{\sqrt{N}\gamma_{j,h}^U-\sqrt{N}}{\sqrt{1-2\gamma_{j,h}^U\rho_{\mathcal{H}_0}^{j,h}+(\gamma_{j,h}^U)^2}}\right). \tag{27b}$$

As a result, the branch threshold (17a) and (17b) can be obtained by inverting (27a) and (27b), respectively. ■

From the derivation above and the expressions of the branch threshold in (17), it is clear that the branch threshold $\gamma_{j,h}^L$ and $\gamma_{j,h}^U$ of the proposed predecision algorithm depends on the number of compressed measurements N, the correlation coefficient $\rho_{\mathcal{H}_0}^{j,h}$ of different channel energies, and the branch target false alarm probability $P_f^{j,h}$ and the way to split the target $P_f^{j,h}$. The correlation coefficient $\rho_{\mathcal{H}_0}^{j,h}$ in (24) only depends on the measurement matrix $\mathbf{A}$ of the MWC. It is important to notice that the branch threshold $\gamma_{j,h}^L$ and $\gamma_{j,h}^U$ are not related to σ_w^2, i.e., the power of the background Gaussian white noise, and no prior knowledge of the PU signal is needed. This is reason why our PCER detector (11) is robust to noise uncertainty.

For the special case that the target branch probability of false alarm is set to be identical for different values of j and h, the overall probability of false alarm P_f in (16a) reduces to

$$P_f = 1-(1-P_f^{j,h})^K. \tag{28}$$

In turn, with the NP criterion along with a targeted overall P_f, the branch decision threshold can be found by inverting (28), splitting $P_f^{j,h}$ and inverting (27).

C. Detection Probability Analysis

Under hypothesis $\mathcal{H}_1$, the input signal $x(t)$ is a sum of the unknown deterministic PU signal $s(t)$ and the Gaussian white noise $w(t)$. To apply (16b) to find the overall probability of detection, we first study the branch probability of detection $P_d^{j,h}$, which is given by Theorem 2 as follows.

Theorem 2: Under hypothesis $\mathcal{H}_1$, the branch probability of detection $P_d^{j,h}$, $j=1,2,\ldots,K$ and $h=j-1$, is expressed as

$$P_d^{j,h} = P_{d,L}^{j,h} + P_{d,U}^{j,h} \tag{29}$$

where $P_{d,L}^{j,h}$ and $P_{d,U}^{j,h}$ are given by (30a) and (30b), respectively, at the bottom of this page, where $\gamma_{j,h}^L$ and $\gamma_{j,h}^U$ have been given in Theorem 1 and $\rho_{\mathcal{H}_1}^{j,h}$ is the correlation coefficient of T_j^{fd} and T_h^{fd} under $\mathcal{H}_1$ which is given by

$$\rho_{\mathcal{H}_1}^{j,h} = \frac{\Sigma+\Theta}{\sqrt{D\left[T_j^{\text{fd}}|\mathcal{H}_1\right] D\left[T_h^{\text{fd}}|\mathcal{H}_1\right]}} \tag{31}$$

where Σ and Θ are defined as

$$\Sigma \triangleq \frac{N\sigma_w^4\left(\rho_0^2+\rho_1^2+\rho_2^2+\rho_3^2\right)}{2} \tag{32a}$$

$$\Theta \triangleq 2\sigma_w^2\left(\eta_j^r\eta_h^i\rho_0+\eta_j^i\eta_h^r\rho_1+\eta_j^r\eta_h^r\rho_2+\eta_j^i\eta_h^i\rho_3\right) \tag{32b}$$

where ρ_0, ρ_1, ρ_2, and ρ_3 are given in Theorem 1, $\eta_j^r = \Re[\sum_{l=-L_0}^{L_0} c_{jl}S(k-lN)]$, $\eta_j^i = \Im[\sum_{l=-L_0}^{L_0} c_{jl}S(k-lN)]$, $\eta_h^r = \Re[\sum_{l=-L_0}^{L_0} c_{hl}S(k-lN)]$, and $\eta_h^i = \Im[\sum_{l=-L_0}^{L_0} c_{hl}S(k-lN)]$, $k=0,1,\ldots,N-1$.

Proof: To prove Theorem 2, we first proceed to find the CDF of $r_{j,h}$ under $\mathcal{H}_1$. Similar to the proof of Theorem 1, we

$$P_{d,L}^{j,h} = \Phi\left(\frac{\gamma_{j,h}^L E\left[T_h^{\text{fd}}|\mathcal{H}_1\right]-E\left[T_j^{\text{fd}}|\mathcal{H}_1\right]}{\sqrt{D\left[T_j^{\text{fd}}|\mathcal{H}_1\right]-2\gamma_{j,h}^L\rho_{\mathcal{H}_1}^{j,h}\sqrt{D\left[T_j^{\text{fd}}|\mathcal{H}_1\right]D\left[T_h^{\text{fd}}|\mathcal{H}_1\right]}+(\gamma_{j,h}^L)^2D\left[T_h^{\text{fd}}|\mathcal{H}_1\right]}}\right) \tag{30a}$$

$$P_{d,U}^{j,h} = 1-\Phi\left(\frac{\gamma_{j,h}^U E\left[T_h^{\text{fd}}|\mathcal{H}_1\right]-E\left[T_j^{\text{fd}}|\mathcal{H}_1\right]}{\sqrt{D\left[T_j^{\text{fd}}|\mathcal{H}_1\right]-2\gamma_{j,h}^U\rho_{\mathcal{H}_1}^{j,h}\sqrt{D\left[T_j^{\text{fd}}|\mathcal{H}_1\right]D\left[T_h^{\text{fd}}|\mathcal{H}_1\right]}+(\gamma_{j,h}^U)^2D\left[T_h^{\text{fd}}|\mathcal{H}_1\right]}}\right) \tag{30b}$$

study the statistic property of the nominator and denominator of the detector $r_{j,h}$ under $\mathcal{H}_1$. Under $\mathcal{H}_1$, the DFT of $y_i(n)$ in the ith channel, $i = 1, 2, \ldots, K,\ n = 0, 1, \ldots, N-1$, can be written as

$$\begin{aligned} Y_i(k) &= \sum_{l=-L_0}^{L_0} c_{il} X(k - lN) \\ &= \sum_{l=-L_0}^{L_0} c_{il} S(k - lN) + \sum_{l=-L_0}^{L_0} c_{il} W(k - lN) \end{aligned} \quad (33)$$

where $S(k-lN)$ and $W(k-lN)$ are sampled from the DTFT of $s(t)$ and $w(t)$, respectively. Lemma 2 given in Appendix B provides the statistics of $|Y_i(k)|^2$, and T_i^{fd} is shown to follow a Gaussian distribution approximately by applying the central limit theorem when N is large. Consequently, the expectation and variance of T_i^{fd} can be derived from Lemma 2 as follows, respectively:

$$E\left[T_i^{\text{fd}}|\mathcal{H}_1\right] = \frac{1}{N}\sum_{k=0}^{N-1}\left|\sum_{l=-L_0}^{L_0} c_{il} S(k - lN)\right|^2 + N\sigma_w^2 \quad (34a)$$

$$D\left[T_i^{\text{fd}}|\mathcal{H}_1\right] = \frac{2\sigma_w^2}{N}\sum_{k=0}^{N-1}\left|\sum_{l=-L_0}^{L_0} c_{il} S(k - lN)\right|^2 + N\sigma_w^4. \quad (34b)$$

The correlation coefficient between T_j^{fd} and T_h^{fd}, by definition, is calculated as

$$\rho_{\mathcal{H}_1}^{j,h} = \frac{\text{Cov}\left[T_j^{\text{fd}}, T_h^{\text{fd}}\right]}{\sqrt{D\left[T_j^{\text{fd}}|\mathcal{H}_1\right] D\left[T_h^{\text{fd}}|\mathcal{H}_1\right]}} \quad (35)$$

where the covariance of T_j^{fd} and T_h^{fd}, according to (51), can be computed as

$$\begin{aligned} \text{Cov}\left[T_j^{\text{fd}}, T_h^{\text{fd}}\right] &= \text{Cov}\left[\frac{1}{N}\sum_{k=0}^{N-1}|Y_j(k)|^2, \frac{1}{N}\sum_{k'=0}^{N-1}|Y_h(k')|^2\right] \\ &= \frac{N\sigma_w^4}{2}\left(\rho_0^2 + \rho_1^2 + \rho_2^2 + \rho_3^2\right) \\ &\quad + 2\sigma_w^2\left(\eta_j^r\eta_h^i\rho_0 + \eta_j^i\eta_h^r\rho_1 + \eta_j^r\eta_h^r\rho_2 + \eta_j^i\eta_h^i\rho_3\right). \end{aligned} \quad (36)$$

Upon obtaining the statistics of T_i^{fd}, and the correlation coefficient of T_j^{fd} and T_h^{fd}, Property 1 is again applied to compute the CDF of $r_{j,h}$ under $\mathcal{H}_1$. Similarly, according to the definition of $P_d^{j,h}$ in (14b), we split $P_d^{j,h}$ into two parts as $P_{d,L}^{j,h}$ and $P_{d,U}^{j,h}$, which satisfy

$$P_{d,L}^{j,h} = \Pr\left(r_{j,h} \le \gamma_{j,h}^L|\mathcal{H}_1\right) \quad (37a)$$

$$P_{d,U}^{j,h} = \Pr\left(r_{j,h} \ge \gamma_{j,h}^U|\mathcal{H}_1\right). \quad (37b)$$

Consequently, with the CDF function of $r_{j,h}$, $P_{d,L}^{j,h}$ and $P_{d,U}^{j,h}$ can be obtained as (30a) and (30b), respectively. ■

With the branch probability of detection $P_d^{j,h}$, $j = 1, 2, \ldots, K,\ h = j-1$, we can compute the overall probability of detection P_d by fusing them as (16b).

IV. Performance Simulation and Discussion

In previous section, we have obtained the false alarm probability P_f, the decision threshold, and the detection probability P_d. Here, we present numerical results to validate the correctness of the theoretical analysis and illustrate the effectiveness of the proposed PCER predecision algorithm.

A. Parameters Setting

In the following simulations, the system parameters are set as follows. The equivalent Nyquist sampling rate $f_{\text{NYQ}} = 600$˜MHz, and the number of sampling channels $K = 20$. The period of $p_i(t)$, $i = 1, 2, \ldots, K$, is $T_p = 75$ ns, containing $M = 45$ chips of ± 1 levels in each period. The sampling rate of a single channel is $f_s = f_p = 1/T_p$, and the cutoff frequency of the LPF in each channel is $f_s/2$. The PU signal consists of three digital modulation signals (i.e., the number of occupied bands is $B = 6$), the symbol rate of each signal is 1˜MBaud, and the carrier frequency of each signal is $l' f_p$, where l' is randomly drawn from the set $\{1, 2, \ldots, L_0\}$ with equal probability. The powers of the three signals are set to be identical, and the signal-to-noise ratio (SNR) is defined as $(P/\sigma_w^2)_{\text{dB}}$, where P is the total power of the PU signals and σ_w^2 is the power spectrum density of the back ground noise $w(t)$. To evaluate the robustness of the proposed detection technique to the variation of the noise level, the noise uncertainty denoted by ρ is also defined. In the presence of noise uncertainty, the value of noise power of each realization uniformly draws from the range of $[\sigma_w^2/\rho, \sigma_w^2\rho]$, where $\rho \ge 1$. And $\rho = 1$ implies that the noise power is fixed as a constant and there is no noise uncertainty. Following the NP criterion, the probability of false alarm P_f is preset as 0.01. Without loss of generality, the branch $P_f^{j,h}$ is split into two equal parts, which means $P_{f,L}^{j,h} = P_{f,U}^{j,h}$. All the simulation results are averaged over 10^5 Monte Carlo experiments.

B. Simulation Results

Fig. 4 presents the detection probability P_d versus SNR of different spectrum sensing methods in the presence/absence of noise uncertainty. The probability of detection of ED is obtained by combining the energy detection results of all the output channels of MWC with the "OR" fusion rule. It shows that the theoretical and simulation results of ED under the case of no noise uncertainty match well with each other. Note that the theoretical result of ED can be obtained by using the statistical distribution of the energy T_i^{fd}, which has been derived before. If introducing the noise uncertainty, i.e., $\rho > 1$, which is commonly seen in practical scenarios, ED suffers a significant performance loss in the detection probability.

For our proposed PCER detector, two sets of curves are provided corresponding to the all-branch fusion rule (13) with simulated results and the partial-branch fusion rule (15) with both theoretical and simulated results, respectively. It can be observed that the all-branch fusion outperforms the partial-branch fusion, since it uses more branch ratios to obtain the final decision at higher complexity. A small gap between the theoretical and simulation results of partial-branch fusion is caused by directly

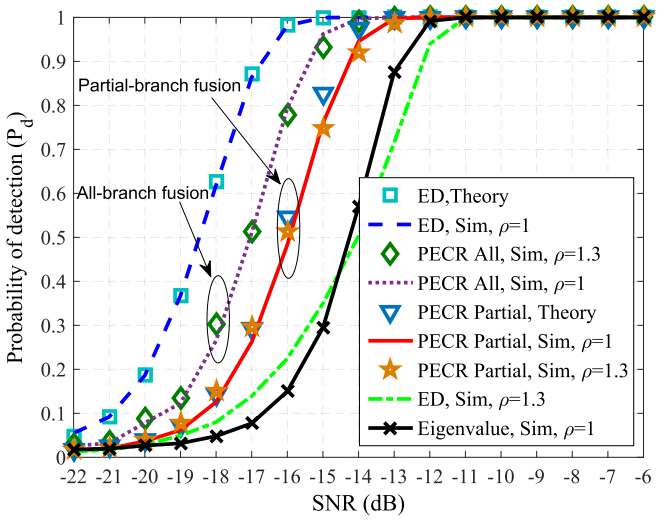

Fig. 4. Probability of detection of different spectrum sensing methods versus SNR.

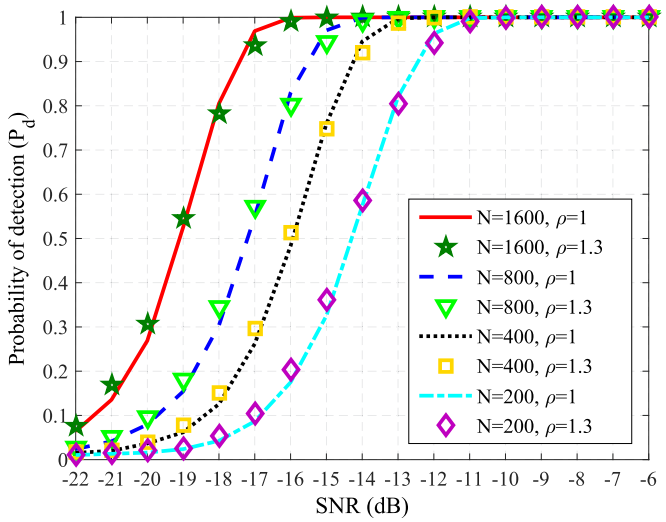

Fig. 5. Probability of detection of PCER of partial-branch fusion rule versus SNR with different N and ρ.

applying the "OR" fusion rule and ignoring the small correlation between the fusion branches. Overall, unlike ED, both all-branch fusion rule and partial-branch fusion rule for PCER detector are robust to noise uncertainty.

The recently introduced eigenvalue-based detector [38] has been modified to fit in the wideband setup. The resulting detector is included in Fig. 4. Specifically, we first use compressed samples to construct the autocorrelation matrix $\mathbf{Q}$ as defined in (6) and then employ the ratio of the maximal eigenvalue to the minimal eigenvalue of $\mathbf{Q}$ as the test statistic. The decision threshold can be approximately computed using the result of [48]. However, different from the conventional eigenvalue detector, which is used in the Nyquist sampling framework, the compressed samples from each channel of MWC are statistically correlated, and the prewhitening technique proposed in [38] is not applicable here. The consequence is that the equivalent number of signal sample has been reduced, which leads to a performance loss.

Various cases of the number of compressed measurements N for partial-branch fusion rule are considered in Fig. 5. The value of N is chosen as 200, 400, 800, and 1600, respectively. It is shown that the proposed PCER detector can achieve good performance with only 200 compressed samples under relatively low SNR, and the detection performance can be promisingly improved by increasing the number of compressed samples. When there exists noise uncertainty, the decision threshold computed by (17) does not change for a given N such that the performance under noise uncertainty is consistent with the case of no noise uncertainty. The results in Fig. 5 further verify our theoretical analysis under different of parameter setups.

The false alarm probability of the PCER detector for the partial-branch fusion rule with various number of compressed measurements N and different values of noise uncertainty ρ is illustrated in Fig. 6. Curves are obtained using the theoretical threshold derived by (17). In Fig. 6, the term "Trial index" represents the number of the independent experiments, and in each experiments, 10^5 Monte Carlo simulations are conducted.

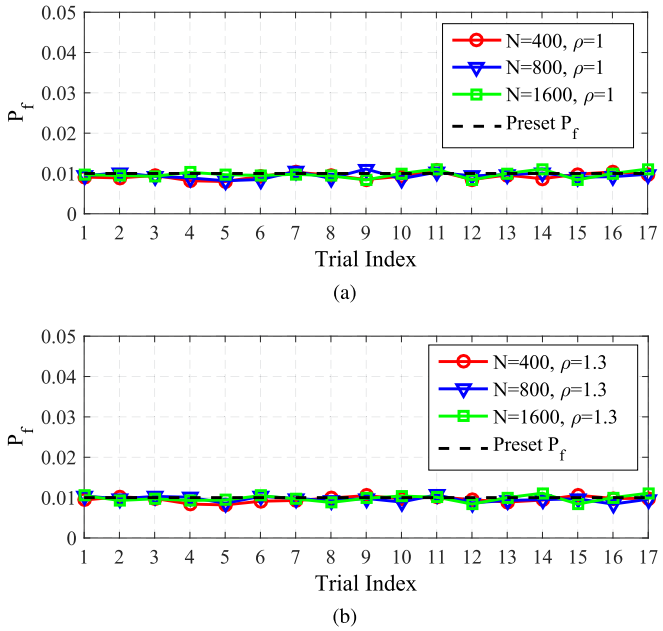

Fig. 6. False alarm probability of the PCER for the partial-branch fusion rule. (a) $\rho = 1$. (b) $\rho = 1.3$.

It is shown that the false alarm probability of the proposed PCER is slightly fluctuating around the preset target value (0.01) under different values of N and ρ, implying the correctness of our derivation.

Fig. 7 presents the receiver operating characteristic (ROC) curves of the PCER detector. The probability of false alarm P_f ranges from 10^{-3} to 10^{-1}, and SNR $= -14$˜dB. It is observed that when there exists noise uncertainty, the performance of the PCER remains nearly unchanged compared with that in the absence of noise uncertainty. From the results presented in Figs. 4–7, it can be concluded that the proposed PCER detection method, which does not require the knowledge of noise power and the PU signals, provides good performance in a wide range of SNR under different parameter setups.

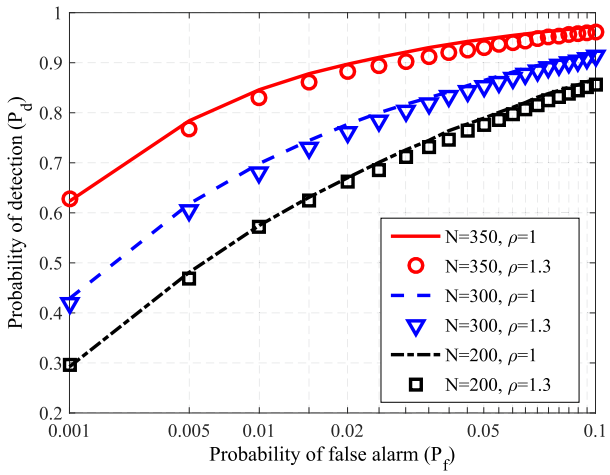

Fig. 7. ROC curves of the PCER.

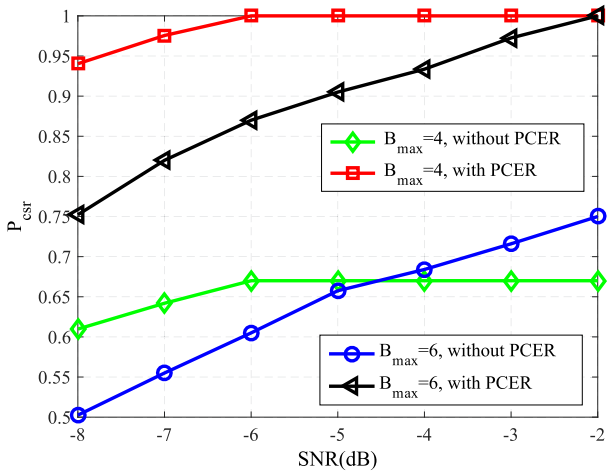

Fig. 8. CSR rate with and without the PCER.

To show the necessity and significance of the proposed PCER detector, we proceed to investigate the correct support recovery (CSR) rate P_{csr} with and without the PCER module, as shown in the Fig. 8. The CSR rate is defined as the ratio of the number of CSR, i.e., $\{\mathbb{S} = \mathbb{S}'\}$, to the total number of simulations. Here, $\mathbb{S}$ and $\mathbb{S}'$ represent the recovery support and the true support of the input signal, respectively. Note that the recovery support $\mathbb{S}$ should be a null set when there is only white noise in the frequency band. With the PCER module, which is inserted between the compressed sampling module and the SR module, the function of SR will be conducted only if the PCER module detects the presence of the PU signals; otherwise, the SR module is bypassed. Without the PCER module, the SR module is always active and output a support set even there is only white noise in the concerned frequency band. Both cases are experimented with the maximum number of occupied band $B_{\max} = [4, 6]$. Once $B_{\max}$ is given, the number of occupied band, which is an even number (including zero), will be equiprobably selected in the range of $[0, B_{\max}]$ in a simulation.

As shown in Fig. 8, P_{csr} with the PCER module outperforms that without the PCER module, where the performance improvement depends on the probability that there are no PU signals in the given wideband. The performance improvement of the proposed SNSS framework over the conventional MWC-based SNSS relies on the accurate detection of PU signals by the PCER module, avoiding the incorrect SR when there is only white noise.

In the aspect of complexity, it needs KN multiplications, $K(N-1)$ additions, and $K(K-1)/2$ divisions for the all-branch fusion rule and only K divisions for the partial-branch fusion rule. However, support recovery requires correlation matrix construction, matrix decomposition, and orthogonal matching pursuit process. Correlation matrix construction needs NK^2 multiplications and $(N-1)K^2$ additions. Matrix decomposition and orthogonal matching pursuit have computational complexity $O(K^3)$ and $O(BLK^2)$, respectively. Therefore, the proposed PCER module can reduce the average computational cost while improving the CSR rate.

V. Conclusion

Based on a MWC framework for SNSS, a predecision detector referred to as the PCER is proposed to determine the presence/absence of PU signals prior to signal SR. The PCER detector utilizes the ratio of pairwise energy from different channels of the MWC as the test statistic, whose CDFs under both $\mathcal{H}_0$ and $\mathcal{H}_1$ have been derived. The decision threshold and the probability of detection under the NP criterion are provided in closed form, which show that the decision threshold is unrelated to the noise power. The theoretical analysis is shown to match well with simulation results under various simulation setups. The proposed PCER detector is observed to offer good detection performance without requiring any prior knowledge of the PU signals in a wide range of SNR. Furthermore, unlike the conventional ED, the PCER detector is robust to the noise uncertainty. Our results indicate that the integration of the PCER detector in the MWC framework can lead to a significant improvement of the CSR rate of the PU signals with low computational cost, making the MWC-based SNSS framework more useful for wideband spectrum sensing.

Appendix A
Lemma 1

Lemma 1: Under $\mathcal{H}_0$, the mean and variance of $|Y_i(k)|^2$ are

$$E\left[|Y_i(k)|^2\right] = N\sigma_w^2 \tag{38a}$$

$$D\left[|Y_i(k)|^2\right] = N^2\sigma_w^4 \tag{38b}$$

respectively, where $i = 1, 2, \ldots, K$, $k = 0, 1, \ldots, N-1$. The covariance of the power spectrum lines $|Y_j(u)|^2$ and $|Y_h(v)|^2$ for different values of (j, h) and (u, v) is

$$\text{Cov}\left[|Y_j(u)|^2, |Y_h(v)|^2\right] = \begin{cases} 0, & j = h, u \neq v \\ \dfrac{N^2\sigma_w^4}{2}\displaystyle\sum_{i'=0}^{3}\rho_{i'}^2, & j \neq h, u = v \\ 0, & j \neq h, u \neq v \end{cases} \tag{39}$$

where $j, h = 1, 2, \ldots, K$, $u, v = 0, 1, \ldots, N-1$, ρ_0, ρ_1, ρ_2, and ρ_3 are defined in Theorem 1.

Proof: Considering the linear property of DFT operation, $X(k-lN)$ under $\mathcal{H}_0$ is a complex Gaussian random variable with zero mean and variance $N\sigma_w^2$. $Y_i\,(k)$, the weighted sum of $X\,(k-lN)$ according to (21), is a complex Gaussian random variable with zero mean and variance $\sum_{l=-L_0}^{L_0}|c_{il}|^2 N\sigma_w^2$. In the MWC system, the power of the periodic ± 1 sequences is unit; therefore, the mean and variance of $Y_i\,(k)$ is computed as $E[Y_i\,(k)]=0$ and $D[Y_i\,(k)]=N\sigma_w^2$, and the mean and variance of $\Re(Y_i(k))$ and $\Im(Y_i(k))$, respectively, are given by

$$E\big[\Re(Y_i(k))\big]=E\big[\Im(Y_i(k))\big]=0 \tag{40a}$$

$$D\big[\Re(Y_i(k))\big]=D\big[\Im(Y_i(k))\big]=N\sigma_w^2/2. \tag{40b}$$

Also note that the covariance of $\Re(X(k))$ and $\Im(X(k))$ is zero [49], and the covariance of $\Re(Y_i(k))$ and $\Im(Y_i(k))$ can be obtained by (41), shown at the bottom of this page.

Thus, $|Y_i(k)|^2=\big[\Re(Y_i(k))\big]^2+\big[\Im(Y_i(k))\big]^2$ is a sum of the squares of two independent and identically distributed Gaussian random variable, and we have

$$E\big[|(Y_i(k))|^2\big]=2\Big(\sqrt{N\sigma_w^2/2}\Big)^2=N\sigma_w^2 \tag{42a}$$

$$D\big[|(Y_i(k))|^2\big]=4\Big(\sqrt{N\sigma_w^2/2}\Big)^4=N^2\sigma_w^4 \tag{42b}$$

which is consistent with (38).

To prove (39), we note that $X(k-lN)$ in (21) is equivalent to the DFT of the compressed samples obtained from $x(t)e^{2\pi l f_s t}$, the frequency-shift version of the original $x(t)$. Therefore, different spectrum lines $X(u-lN)$ and $X(v-lN)$, $u\neq v$, shifted from the same frequency band are uncorrelated [49], and the spectrum lines $X(u-lN)$ and $X(v-l'N)$, $l\neq l'$, are also uncorrelated, since the samples used to compute DFT are obtained from different narrow band white noise under $\mathcal{H}_0$, which means $\mathrm{Cov}\,[Y_j\,(u),Y_h\,(v)]=0$, $j=h$, $u\neq v$. Meanwhile, $|Y_j(u)|^2$ and $|Y_h(v)|^2$ are continuous functions of $Y_j(u)$ and $Y_h(v)$, respectively, implying

$$\mathrm{Cov}\left[|Y_j\,(u)|^2,|Y_h\,(v)|^2\right]=0 \tag{43}$$

where $j=h$ and $u\neq v$.

To compute the covariance of $|Y_j(u)|^2$ and $|Y_h(v)|^2$ for $j\neq h$ and $u=v$, we first determine the following four items: $\mathrm{Cov}\big[\Re(Y_j(u)),\Re(Y_h(v))\big]$, $\mathrm{Cov}\big[\Re(Y_j(u)),\Im(Y_h(v))\big]$, $\mathrm{Cov}\big[\Im(Y_j(u)),\Re(Y_h(v))\big]$, $\mathrm{Cov}\big[\Im(Y_j(u)),\Im(Y_h(v))\big]$, where $\mathrm{Cov}\big[\Re(Y_j(u)),\Re(Y_h(v))\big]$ is computed by (44), shown at the bottom of the page. The other three items can be computed in the same fashion.

Using the result of (40), the correlation coefficient of $\Re(Y_p(k))$ and $\Re(Y_q(k))$ can be obtained as ρ_2; thus, the correlation coefficient of $[\Re(Y_p(k))]^2$ and $[\Re(Y_q(k))]^2$ is ρ_2^2 [50]. Consequently

$$\begin{aligned}&\mathrm{Cov}\left[\left[\Re\left(Y_j\,(u)\right)\right]^2,\left[\Re\left(Y_h\,(v)\right)\right]^2\right]\\&=\rho_2^2\sqrt{D\left[\left[\Re\left(Y_j\,(u)\right)\right]^2\right]D\left[\left[\Re\left(Y_h\,(v)\right)\right]^2\right]}\\&=\frac{N^2\sigma_w^4}{2}\rho_2^2.\end{aligned} \tag{45}$$

Similarly, we have

$$\mathrm{Cov}\left[\left[\Re\left(Y_j\,(u)\right)\right]^2,\left[\Im\left(Y_h\,(v)\right)\right]^2\right]=\frac{N^2\sigma_w^4}{2}\rho_0^2 \tag{46a}$$

$$\mathrm{Cov}\left[\left[\Im\left(Y_j\,(u)\right)\right]^2,\left[\Re\left(Y_h\,(v)\right)\right]^2\right]=\frac{N^2\sigma_w^4}{2}\rho_1^2 \tag{46b}$$

$$\mathrm{Cov}\left[\left[\Im\left(Y_j\,(u)\right)\right]^2,\left[\Im\left(Y_h\,(v)\right)\right]^2\right]=\frac{N^2\sigma_w^4}{2}\rho_3^2. \tag{46c}$$

$$\begin{aligned}&\mathrm{Cov}\big[\Re(Y_i(k)),\Im(Y_i(k))\big]=E\big[\Re(Y_i(k))\Im(Y_i(k))\big]-E\big[\Re(Y_i(k))\big]E\big[\Im(Y_i(k))\big]\\&=E\left[\left(\sum_{l=-L_0}^{L_0}\left(\Re\left(c_{il}\right)\Re\left(X\left(k-lN\right)\right)-\Im\left(c_{il}\right)\Im\left(X\left(k-lN\right)\right)\right)\right)\right.\\&\quad\left.\times\left(\sum_{l=-L_0}^{L_0}\left(\Re\left(c_{il}\right)\Im\left(X\left(k-lN\right)\right)+\Im\left(c_{il}\right)\Re\left(X\left(k-lN\right)\right)\right)\right)\right]\\&=0.\end{aligned} \tag{41}$$

$$\begin{aligned}&\mathrm{Cov}\big[\Re(Y_j(u)),\Re(Y_h(v))\big]=E\big[\Re(Y_j(u))\Re(Y_h(v))\big]-E\big[\Re(Y_j(u))\big]E\big[\Re(Y_h(v))\big]\\&=E\left[\left(\sum_{l=-L_0}^{L_0}\left(\Re\left(c_{jl}\right)\Re\left(X\left(u-lN\right)\right)-\Im\left(c_{jl}\right)\Im\left(X\left(u-lN\right)\right)\right)\right)\right.\\&\quad\left.\times\left(\sum_{l=-L_0}^{L_0}\left(\Re\left(c_{hl}\right)\Re\left(X\left(v-lN\right)\right)-\Im\left(c_{hl}\right)\Im\left(X\left(v-lN\right)\right)\right)\right)\right]\\&=\sum_{l=-L_0}^{L_0}\Re\left(c_{jl}\right)\Re\left(c_{hl}\right)\frac{\sigma_w^2}{2}+\sum_{l=-L_0}^{L_0}\Im\left(c_{jl}\right)\Im\left(c_{hl}\right)\frac{\sigma_w^2}{2}=\frac{N\sigma_w^2\rho_2}{2}.\end{aligned} \tag{44}$$

With (45) and (46), the covariance of $|Y_j(u)|^2$ and $|Y_h(v)|^2$ is computed as

$$\mathrm{Cov}\left[|Y_j(u)|^2, |Y_h(v)|^2\right] = \frac{N^2\sigma_w^4\left(\rho_0^2+\rho_1^2+\rho_2^2+\rho_3^2\right)}{2} \tag{47}$$

where $j \neq h$ and $u = v$.

For the case $j \neq h$ and $u \neq v$, in the same process, it is easy to obtain

$$\mathrm{Cov}\left[\left[\Re\left(Y_j(u)\right)\right]^2, \left[\Re\left(Y_h(v)\right)\right]^2\right] = 0 \tag{48a}$$

$$\mathrm{Cov}\left[\left[\Re\left(Y_j(u)\right)\right]^2, \left[\Im\left(Y_h(v)\right)\right]^2\right] = 0 \tag{48b}$$

$$\mathrm{Cov}\left[\left[\Im\left(Y_j(u)\right)\right]^2, \left[\Re\left(Y_h(v)\right)\right]^2\right] = 0 \tag{48c}$$

$$\mathrm{Cov}\left[\left[\Im\left(Y_j(u)\right)\right]^2, \left[\Im\left(Y_h(v)\right)\right]^2\right] = 0 \tag{48d}$$

which leads to

$$\mathrm{Cov}\left[|Y_j(u)|^2, |Y_h(v)|^2\right] = 0 \tag{49}$$

where $j \neq h$ and $u \neq v$. With (43), (47), and (49), we can derive (39) in Lemma 1. ■

Appendix B
Lemma 2

Lemma 2: Under $\mathcal{H}_1$, the mean and variance of $|Y_i(k)|^2$ are

$$E\left[|Y_i(k)|^2\right] = \left|\sum_{l=-L_0}^{L_0} c_{il}S(k-lN)\right|^2 + N\sigma_w^2 \tag{50a}$$

$$D\left[|Y_i(k)|^2\right] = 2N\sigma_w^2\left|\sum_{l=-L_0}^{L_0} c_{il}S(k-lN)\right|^2 + N^2\sigma_w^4 \tag{50b}$$

respectively, where $i = 1, 2, \ldots, K$, $k = 0, 1, \ldots, N-1$. The covariance of spectrum lines $|Y_j(u)|^2$ and $|Y_h(v)|^2$ for different values of (j, h) and (u, v) is

$$\mathrm{Cov}\left[|Y_j(u)|^2, |Y_h(v)|^2\right] = \begin{cases} 0, & j = h, u \neq v \\ N(\Sigma+\Theta), & j \neq h, u = v \\ 0, & j \neq h, u \neq v \end{cases} \tag{51}$$

where $j,\ h = 1, 2, \ldots, K,\ u,\ v = 0, 1, \ldots, N-1$, and Σ and Θ are defined by (32a) and (32b), respectively.

Proof: The proof of Lemma 2 is similar with that of Lemma 1 if we follow the assumption that $s(t)$ under $\mathcal{H}_1$ is a deterministic signal. ■

References

[1] S. Yin, D. Chen, Q. Zhang, M. Liu, and S. Li, "Mining spectrum usage data: A large-scale spectrum measurement study," *IEEE Trans. Mobile Comput.*, vol. 11, no. 6, pp. 1033–1046, Jun. 2012.

[2] A. Al-Hourani, V. Trajkovic, S. Chandrasekharan, and S. Kandeepan, "Spectrum occupancy measurements for different urban environments," in *Eur. Conf. Proc. Netw. Commun.*, Jun. 2015, pp. 97–102.

[3] Y. Chen and H. S. Oh, "A survey of measurement-based spectrum occupancy modeling for cognitive radios," *IEEE Commun. Surveys Tuts.*, vol. 18, no. 1, pp. 848–859, First Quarter 2016.

[4] S. Haykin, "Cognitive radio: Brain-empowered wireless communications," *IEEE J. Sel. Areas Commun.*, vol. 23, no. 2, pp. 201–220, Feb. 2005.

[5] J. Wang, M. Ghosh, and K. Challapali, "Emerging cognitive radio applications: A survey," *IEEE Commun. Mag.*, vol. 49, no. 3, pp. 74–81, Mar. 2011.

[6] Y. Zeng and Y. C. Liang, "Spectrum-sensing algorithms for cognitive radio based on statistical covariances," *IEEE Trans. Veh. Technol.*, vol. 58, no. 4, pp. 1804–1815, May 2009.

[7] E. Axell, G. Leus, E. G. Larsson, and H. V. Poor, "Spectrum sensing for cognitive radio: State-of-the-art and recent advances," *IEEE Signal Process. Mag.*, vol. 29, no. 3, pp. 101–116, May 2012.

[8] V. M. Patil and S. R. Patil, "A survey on spectrum sensing algorithms for cognitive radio," in *Proc. Int. Conf. Adv. Human Mach. Interact.*, Mar. 2016, pp. 1–5.

[9] P. Wang, J. Fang, N. Han, and H. Li, "Multiantenna-assisted spectrum sensing for cognitive radio," *IEEE Trans. Veh. Technol.*, vol. 59, no. 4, pp. 1791–1800, May 2010.

[10] H. Sun, A. Nallanathan, C. X. Wang, and Y. Chen, "Wideband spectrum sensing for cognitive radio networks: A survey," *IEEE Wireless Commun.*, vol. 20, no. 2, pp. 74–81, Apr. 2013.

[11] D. Bao, L. D. Vito, and S. Rapuano, "A histogram-based segmentation method for wideband spectrum sensing in cognitive radios," *IEEE Trans. Instrum. Meas.*, vol. 62, no. 7, pp. 1900–1908, Jul. 2013.

[12] Z. Zeinalkhani and A. H. Banihashemi, "Ultra low-complexity detection of spectrum holes in compressed wideband spectrum sensing," in *Proc. IEEE Global Commun. Conf.*, Dec. 2015, pp. 1–7.

[13] Z. Qin, Y. Gao, M. D. Plumbley, and C. G. Parini, "Wideband spectrum sensing on real-time signals at sub-Nyquist sampling rates in single and cooperative multiple nodes," *IEEE Trans. Signal Process.*, vol. 64, no. 12, pp. 3106–3117, Jun. 2016.

[14] S. Hoyos, B. M. Sadler, and G. R. Arce, "Monobit digital receivers for ultrawideband communications," *IEEE Trans. Wireless Commun.*, vol. 4, no. 4, pp. 1337–1344, Jul. 2005.

[15] S. K. Sharma, E. Lagunas, S. Chatzinotas, and B. Ottersten, "Application of compressive sensing in cognitive radio communications: A survey," *IEEE Commun. Surveys Tuts.*, vol. 18, no. 3, pp. 1838–1860, Third Quarter 2016.

[16] H. Sun, W. Y. Chiu, and A. Nallanathan, "Adaptive compressive spectrum sensing for wideband cognitive radios," *IEEE Commun. Lett.*, vol. 16, no. 11, pp. 1812–1815, Nov. 2012.

[17] D. L. Donoho, "Compressed sensing," *IEEE Trans. Inf. Theory*, vol. 52, no. 4, pp. 1289–1306, Apr. 2006.

[18] E. J. Candes and M. B. Wakin, "An introduction to compressive sampling," *IEEE Signal Process. Mag.*, vol. 25, no. 2, pp. 21–30, Mar. 2008.

[19] Z. Tian and G. B. Giannakis, "Compressed sensing for wideband cognitive radios," in *Proc. IEEE Int. Conf. Acoust., Speech Signal Process.*, Apr. 2007, vol. 4, pp. IV-1357–IV-1360.

[20] J. Jiang, H. Sun, D. Baglee, and H. V. Poor, "Achieving autonomous compressive spectrum sensing for cognitive radios," *IEEE Trans. Veh. Technol.*, vol. 65, no. 3, pp. 1281–1291, Mar. 2016.

[21] Z. Qin, Y. Gao, and C. G. Parini, "Data-assisted low complexity compressive spectrum sensing on real-time signals under sub-Nyquist rate," *IEEE Trans. Wireless Commun.*, vol. 15, no. 2, pp. 1174–1185, Feb. 2016.

[22] S. Kirolos *et al.*, "Analog-to-information conversion via random semodulation," in *Proc. IEEE Dallas/CAS Workshop Des., Appl., Integr. Softw.*, Oct. 2006, pp. 71–74.

[23] J. N. Laska, S. Kirolos, M. F. Duarte, T. S. Ragheb, R. G. Baraniuk, and Y. Massoud, "Theory and implementation of an analog-to-information converter using random demodulation," in *Proc. IEEE Int. Symp. Circuits Syst.*, May 2007, pp. 1959–1962.

[24] J. A. Tropp, J. N. Laska, M. F. Duarte, J. K. Romberg, and R. G. Baraniuk, "Beyond Nyquist: Efficient sampling of sparse bandlimited signals," *IEEE Trans. Inf. Theory*, vol. 56, no. 1, pp. 520–544, Jan. 2010.

[25] X. Chen, Z. Yu, S. Hoyos, B. M. Sadler, and J. Silva-Martinez, "A sub-Nyquist rate sampling receiver exploiting compressive sensing," *IEEE Trans. Circuits Syst. I, Reg. Papers*, vol. 58, no. 3, pp. 507–520, Mar. 2011.

[26] D. D. Arianandа and G. Leus, "Wideband power spectrum sensing using sub-Nyquist sampling," in *Proc. IEEE 12th Int. Workshop Signal Process. Adv. Wireless Commun.*, Jun. 2011, pp. 101–105.

[27] Y. L. Polo, Y. Wang, A. Pandharipande, and G. Leus, "Compressive wideband spectrum sensing," in *Proc. IEEE Int. Conf. Acoust., Speech Signal Process.*, Apr. 2009, pp. 2337–2340.

[28] Y. Wang, A. Pandharipande, Y. L. Polo, and G. Leus, "Distributed compressive wide-band spectrum sensing," in *Proc. Inf. Theory Appl. Workshop*, Feb. 2009, pp. 178–183.
[29] Y. Wang, Z. Tian, and C. Feng, "Sparsity order estimation and its application in compressive spectrum sensing for cognitive radios," *IEEE Trans. Wireless Commun.*, vol. 11, no. 6, pp. 2116–2125, Jun. 2012.
[30] M. Mishali and Y. C. Eldar, "From theory to practice: Sub-Nyquist sampling of sparse wideband analog signals," *IEEE J. Sel. Topics Signal Process.*, vol. 4, no. 2, pp. 375–391, Apr. 2010.
[31] C. Herley and P. W. Wong, "Minimum rate sampling and reconstruction of signals with arbitrary frequency support," *IEEE Trans. Inf. Theory*, vol. 45, no. 5, pp. 1555–1564, Jul. 1999.
[32] R. Venkataramani and Y. Bresler, "Perfect reconstruction formulas and bounds on aliasing error in sub-Nyquist nonuniform sampling of multiband signals," *IEEE Trans. Inf. Theory*, vol. 46, no. 6, pp. 2173–2183, Sep. 2000.
[33] M. Mishali and Y. C. Eldar, "Blind multiband signal reconstruction: Compressed sensing for analog signals," *IEEE Trans. Signal Process.*, vol. 57, no. 3, pp. 993–1009, Mar. 2009.
[34] M. Mishali, Y. C. Eldar, O. Dounaevsky, and E. Shoshan, "Xampling: Analog to digital at sub-Nyquist rates," *IET Circuits, Devices Syst.*, vol. 5, no. 1, pp. 8–20, Jan. 2011.
[35] M. Mishali and Y. C. Eldar, "Wideband spectrum sensing at sub-Nyquist rates [applications corner]," *IEEE Signal Process. Mag.*, vol. 28, no. 4, pp. 102–135, Jul. 2011.
[36] R. B. Bacchus, A. J. Fertner, C. S. Hood, and D. A. Roberson, "Long-term, wide-band spectral monitoring in support of dynamic spectrum access networks at the IIT spectrum observatory," in *Proc. 3rd IEEE Symp. New Frontiers Dyn. Spectrum Access Netw.*, Oct. 2008, pp. 1–10.
[37] R. Tandra and A. Sahai, "SNR walls for signal detection," *IEEE J. Sel. Topics Signal Process.*, vol. 2, no. 1, pp. 4–17, Feb. 2008.
[38] Y. Zeng and Y. C. Liang, "Eigenvalue-based spectrum sensing algorithms for cognitive radio," *IEEE Trans. Commun.*, vol. 57, no. 6, pp. 1784–1793, Jun. 2009.
[39] P. D. Sutton, K. E. Nolan, and L. E. Doyle, "Cyclostationary signatures for rendezvous in OFDM-based dynamic spectrum access networks," in *Proc. 2nd IEEE Int. Symp. New Frontiers Dyn. Spectrum Access Netw.*, Apr. 2007, pp. 220–231.
[40] M. Sun, C. Zhao, S. Yan, and B. Li, "A novel spectrum sensing for cognitive radio networks with noise uncertainty," *IEEE Trans. Veh. Technol.*, 2016, to be published.
[41] A. Mariani, A. Giorgetti, and M. Chiani, "Effects of noise power estimation on energy detection for cognitive radio applications," *IEEE Trans. Commun.*, vol. 59, no. 12, pp. 3410–3420, Dec. 2011.
[42] M. Jin, Q. Guo, J. Tong, J. Xi, and Y. Li, "Energy detection of DVB-T signals against noise uncertainty," *IEEE Commun. Lett.*, vol. 18, no. 10, pp. 1831–1834, Oct. 2014.
[43] D. M. Martnez and G. Andrade, "On the reduction of the noise uncertainty effects in energy detection for spectrum sensing in cognitive radios," in *Proc. IEEE 25th Annu. Int. Symp. Pers., Indoor, Mobile Radio Commun.*, Sep. 2014, pp. 1975–1979.
[44] S. Maleki, S. P. Chepuri, and G. Leus, "Optimal hard fusion strategies for cognitive radio networks," in *Proc. IEEE Wireless Commun. Netw. Conf.*, Mar. 2011, pp. 1926–1931.
[45] F. C. Ribeiro, M. L. R. de Campos, and S. Werner, "Distributed cooperative spectrum sensing with adaptive combining," in *Proc. IEEE Int. Conf. Acoust., Speech Signal Process.*, Mar. 2012, pp. 3557–3560.
[46] K. Cichon, A. Kliks, and H. Bogucka, "Energy-efficient cooperative spectrum sensing: A survey," *IEEE Commun. Surveys Tuts.*, vol. 18, no. 3, pp. 1861–1886, Third Quarter 2016.
[47] D. V. Hinkley, "On the ratio of two correlated normal random variables," *Biometrika*, vol. 56, no. 3, pp. 635–639, 1969.
[48] S. Konishi, "Asymptotic expansion for the distribution of a function of latent roots of the covariance matrix," *Ann. Inst. Statist. Math.*, vol. 29, no. 1, pp. 389–396, 1977.
[49] Q. Pei-Han, L. Zan, S. Jiang-Bo, and G. Rui, "A robust power spectrum split cancellation-based spectrum sensing method for cognitive radio systems," *Chin. Phys. B*, vol. 23, no. 12, pp. 533–543, 2014.
[50] A. H. Joarder, "Moments of the product and ratio of two correlated Chi-square variables," *Statist. Papers*, vol. 50, no. 3, pp. 581–592, 2009.

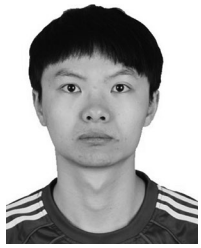

Tianyi Xiong (S'15–M'16) was born in Sichuan Province, China, in 1989. He received the B.S. degree in optical information science and technology from South China University of Technology, Guangzhou, China, in 2011. He is currently working toward the Ph.D. degree at the School of Telecommunications Engineering, Xidian University, Xi'an, China.

His research interests include wireless communication, spectrum sensing, and cognitive radio networks.

Hongbin Li (M'99–SM'08) received the B.S. and M.S. degrees from the University of Electronic Science and Technology of China, Chengdu, China, in 1991 and 1994, respectively, and the Ph.D. degree from the University of Florida, Gainesville, FL, USA, in 1999, all in electrical engineering.

From July 1996 to May 1999, he was a Research Assistant with the Department of Electrical and Computer Engineering, University of Florida. Since July 1999, he has been with the Department of Electrical and Computer Engineering, Stevens Institute of Technology, Hoboken, NJ, USA, where he became a Professor in 2010. He was a Summer Visiting Faculty Member at the Air Force Research Laboratory in the summers of 2003, 2004, and 2009. His general research interests include statistical signal processing, wireless communications, and radars.

Dr. Li is a member of Tau Beta Pi and Phi Kappa Phi. He was the recipient of the IEEE Jack Neubauer Memorial Award in 2013 from the IEEE Vehicular Technology Society, the Outstanding Paper Award from the IEEE AFICON Conference in 2011, the Harvey N. Davis Teaching Award in 2003, the Jess H. Davis Memorial Award for Excellence in Research in 2001 from Stevens Institute of Technology, and the Sigma Xi Graduate Research Award from the University of Florida in 1999. He has been a member of the IEEE Signal Processing Society (SPS) Signal Processing Theory and Methods Technical Committee (TC) and the IEEE SPS Sensor Array and Multichannel TC, an Associate Editor for *Signal Processing* (Elsevier), the IEEE TRANSACTIONS ON SIGNAL PROCESSING, IEEE SIGNAL PROCESSING LETTERS, and the IEEE TRANSACTIONS ON WIRELESS COMMUNICATIONS, and a Guest Editor for the IEEE JOURNAL OF SELECTED TOPICS IN SIGNAL PROCESSING and the *EURASIP Journal on Applied Signal Processing*. He has been involved in various conference organization activities, including serving as a General co-Chair for the 7th IEEE Sensor Array and Multichannel Signal Processing Workshop, Hoboken, NJ, USA, June 17–20, 2012.

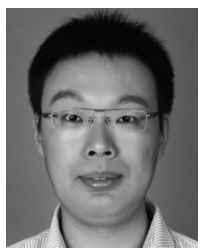

Peihan Qi was born in Henan Province, China, in 1986. He received the B.S. degree in telecommunications engineering from Changan University, Xi'an, China, in 2006, and the M.S. degree in communication and information system and Ph.D. degree in military communication from Xidian University, Xi'an, in 2011 and 2014, respectively.

Since January 2015, he has been a Postdoctoral Researcher with the School of Telecommunications Engineering, Xidian University. His research interests include compressed sensing, spectrum sensing in cognitive radio networks, and high-speed digital signal processing.

Zan Li (SM'14) was born in Shaanxi Province, China, in 1975. She received the B.S. degree in telecommunications engineering and M.S. and Ph.D. degrees in communication and information system from Xidian University, Xi'an, China, in 1988, 2001, and 2006, respectively.

She is a Professor with the School of Telecommunications Engineering, Xidian University. Her research interests include wireless communication system, cognitive radio networks, and digital signal processing.

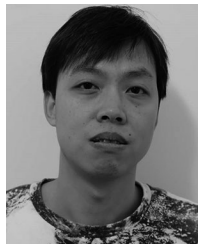

Shilian Zheng (M'11) received the B.S. degree in telecommunications engineering and the M.S. degree in signal and information processing from Hangzhou Dianzi University, Hangzhou, China, in 2005 and 2008, respectively, and the Ph.D. degree in information and communications engineering from Xidian University, Xi'an, China, in 2014.

His current research interests include cognitive radio, compressed sensing, and big data analytics.